International Journal of GEOMATE, July, 2020, Vol.19, Issue 71, pp. 242 - 249
ISSN: 2186-2982 (P), 2186-2990 (O), Japan, DOI: https://doi.org/10.21660/2020.71.96640
Geotechnique, Construction Materials and Environment

AUTOMATIC IMAGE RECOGNITION OF PAVEMENT DISTRESS FOR IMPROVING PAVEMENT INSPECTION

*Min Che Ho[1], Jyh Dong Lin[2] and Chih Fong Huang[3]

[1]Department of Civil Environment Engineering, Hiroshima University, Japan
[2]Department of Civil Engineering, National Central University, Taiwan
[3]Department of Civil Engineering, National Central University, Taiwan

*Corresponding Author, Received: 24 Dec. 2019, Revised: 24 Feb. 2020, Accepted: 11 March 2020

ABSTRACT: Frequent road inspections are key to maintaining road quality and avoiding casualties associated with poor road conditions. In Taiwan, open contractors conduct inspections of roads and ancillary facilities daily or weekly according to the requirements of the agency awarding the contracts. Unfortunately, the equipment used for inspections the inspection data lacks follow-up applications and numerical conversions, such as the Pavement Condition Index (*PCI*), to compile a large-scale database to facilitate the long-term conservation of roads. In this study, this paper developed back-end image recognition software using existing road inspection methods and existing equipment. This was aimed at enhancing inspection efficiency by enabling the automatic identification of road damage. Resulting observations can then be converted into PCI values in accordance with ASTM D6433-16 to be exported as a numeric value indicative of road quality. A vehicle-mounted traffic recorder and imaging device with Wi-Fi transmission capability are used as hardware, and the relationship between the captured images and the speed of the car is used to obtain an accurate indication of road conditions across the surface. The simple linear iterative clustering (SLIC) Superpixels algorithm is used to identify areas with pavement damage as patches, potholes, longitudinal cracking, and crocodile cracking. The results of the proposed fully-automated method conform strongly with those obtained using semi-automated pavement inspection software. Despite the restrictions imposed by the limited depth measurement of 2D images, our method achieved results close to those obtained using manual inspection. Future developments will include the application of artificial intelligence to enhance the effectiveness of this software.

Keywords: Pavement distress, PCI, Automatic image recognition

1. INTRODUCTION

The Construction and Planning Department of the Ministry of the Interior in Taiwan has adopted the pavement condition index (PCI) described in ASTM D6433-11 [1] as the primary index for monitoring pavement conditions [2]. Unfortunately, PCI inspections are time-consuming and laborious, and the current inspection method relies on contractors recording pavement distress types in PCI numerical format. This makes it difficult to apply data collected during inspections to the calculation of PCI values or to make a long-term pavement maintenance plans [3]. This study held the following five objectives: 1) improve road inspection methods using the superpixels method for automated recognition of distress signs; 2) develop software based on the superpixels method to facilitate pavement distress recognition; 3) use clustering to extract indicators of distress from images; 4) develop automatic road inspection software capable of capturing and analyzing images covering the expanse of pavement; 5) compare our fully-automated inspection method with semi-automated methods and conventional manual pavement inspection in terms of cost and efficiency.

The current (semi-automated) road inspection method developed by National Central University relies on visual inspections of images captured at a spacing of 25 m for the recognition of distress signs. Specially trained engineers input the captured images and determine the severity of the distress, whereupon the software calculates the scope of the distress and assigns a PCI value for each 100-meter section of roadway. This method is based on grayscale images using a set threshold value obtained from the average grayscale value of every pixel or segment in the image [4]. Nonetheless, additional image processing techniques are also required to differentiate signs of distress from traffic markers, shadows, and corrupted images. The disadvantage of this method is the fact that it processes only grayscale values; i.e., it disregards other information from the original image [1,5]. Removing arbitrary distractions from images while retaining signs can be exceedingly difficult, particularly in cases where the pavement images are homogeneous. Multiple filtering methods must be employed to extract information from the images, thereby making it nearly impossible to conduct automatic inspections based on this method [6].

2. PAVEMENT IMAGE RECOGNITION

Our primary objective in this research was to improve the quality of the road inspection methods currently used by contractors. The equipment used for road inspections includes an inspection vehicle, a driving recorder, and GPS vehicle trajectory recorder. This paper developed software for the automated identification of pavement distress from captured images of roads. This process involves capturing and processing images followed by analysis. The image capture system provides sufficient resolution to improve on the accuracy of exiting systems. The primary analysis method used in this study was the SLIC superpixels algorithm, which is based on lab pixel analysis, K-means pixel clustering, and distress identification. Superpixels analysis is more efficient than conventional binary image thresholding in terms of identifying pavement distress. A flowchart of the study is presented in Fig. 1.

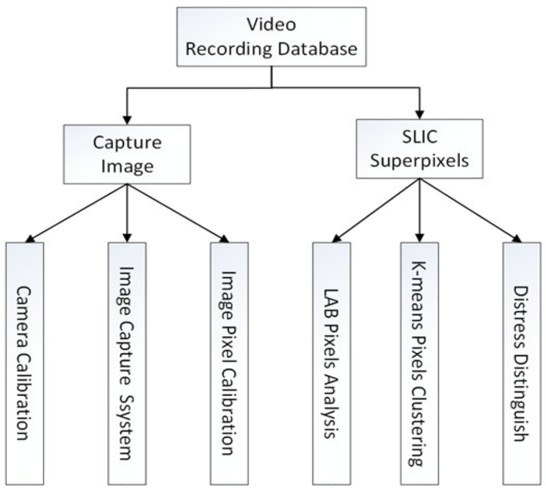

Fig.1 Flow Chart

2.1 Equipment and Database

Three cameras were used in this study: two inexpensive dash cams (RadiQ R32 and ONPRO GT-Z01). The RadiQ R32 provides superior performance in terms of image sensing and resolution; however, it lacks a GPS system. The ONPRO GT-Z01 provides GPS capability. Even these inexpensive devices provide high video resolution. Data was collected from four types of road: a high-speed freeway with no motorcycle access (presumed to have pavement conditions with the highest quality), a freeway that allows large motorcycles (second highest quality), a provincial road similar to a city street but with a higher speed limit (third highest quality), and a city road (lowest quality).

The authors first obtained video recordings of pavement conditions in the form of consecutive images appearing at a set frequency expressed in frames per second (fps). The human visual system is able to process and individually perceive 10 to 12 images per second. Higher frame rates are perceived as motion. Most modern video cameras feature frame rates of 30 fps to 240 fps and most dash cams record video at 30 fps to 60 fps. Under a set frame rate, the driving speed determines the distance between images. Fig. 1 indicates the distance between images at various speeds and frame rates. At a speed of 80 km/h and recording frequency of 15 fps, the distance traveled between images is 1.5 m. Facilitating inspection of the entire road while reducing computational overhead requires minimizing the number of images necessary for a complete survey. For example, 6 fps would be the minimum number of images required for a complete survey at 80 km/h, whereas 4 fps would be required at 40km/h. In this study, this paper assumed that the speed limit on National Freeways is 90 km/h, the speed limit on urban roads is 50 km/h, and the width of the selected area is 4 meters. Thus, this paper adopted a frame rate of 6 fps for national freeways and 4 fps for urban roads.

2.2 Inspection of Pavement Conditions

In this study, the researchers conducted manual inspections of a section of Taiwan National Freeway No. 3 from km 83 to km 89. This paper also conducted inspections on sections of urban roads in order to formulate an accurate indication of the quantity and severity of damage throughout the road sections. Manual inspection of pavement conditions is considered the most accurate method; however, it is time-consuming and expensive. This is the reason that inspections based on the PCI focus on specific areas of the road [7]. Manual inspection allows the extraction of 19 types of distress, including data pertaining to length and depth. National Central University has developed a semi-automated system for the inspection of pavement conditions, wherein an encoder records a road image every 20 m from a camera based on GPS coordinates. An engineer attempts to identify the various types of distress including severity and scope but excluding depth, whereas software is used to calculate the PCI according to the scope of the distress. In this study, This case compared the performance of manual, semi-automated, and fully-automated pavement condition inspection methods.

2.3 Automatic Image Recognition and Image Preprocessing

Our objective in this study was to develop software for the automated analysis of pavement conditions using conventional equipment. A dash cam would be the most practical; however, the captured images would include a lot of detail unnecessary to distress analysis. This means that the images would have to undergo preprocessing, including camera calibration, analysis range selection, and image pixel calibration. Calculating accurate PCI values requires precise distress data, including the type of distress, the area, and the severity. Thus, images captured from video files must be calibrated according to the angle of view, the vertical distance from the road, and the image distortion imposed by the wide angle lens, as shown in Figs. 2 and 3. Following image calibration, the pixels in the image provide an accurate indication of the damage to the pavement.

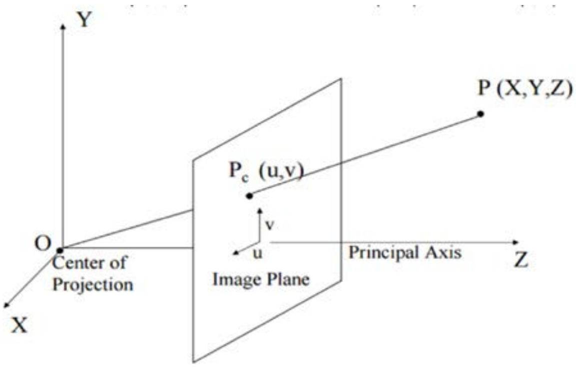

Fig.2 Camera Calibration Theories

$$\begin{pmatrix} u \\ v \\ w \end{pmatrix} = \begin{pmatrix} f & 0 & t_u \\ 0 & f & t_u \\ 0 & 0 & 1 \end{pmatrix} \begin{pmatrix} X \\ Y \\ Z \end{pmatrix}$$

Fig.3 Calibration Matrixes

This paper set the coordinate system $\Omega_1(X, Y, Z) \in R^3$ in the center of the camera focus O, and Z-axis perpendicular to the object surface Π_1. The rays coming from the circle Γ_1 form a skewed cone on surface Π_1, the boundary curve C of which can be expressed as follows:

$$(X - \alpha Z)^2 + (Y - \beta Z)^2 = \gamma^2 Z^2$$

Parameters α and β specify the skewness of the cone in X and Y directions, whereas parameter γ specifies the sharpness of the cone. Thus, if the distance from the camera focus to the object surface is denoted by d, then the circle equation becomes $(X - \alpha d)^2 + (Y - \beta d)^2 = (\gamma d)^2$.

The camera coordinate system $\Omega_2(X, Y, Z) \in R^3$ is also centered in the camera focus; however, the Z-axis is orthogonal to the image plane Π_2, and the x- and y-axes are parallel to image axes u and v. Thus, the transformation from Ω_2 to Ω_1 can be expressed using the following rotation:

$$\begin{pmatrix} X \\ Y \\ Z \end{pmatrix} = \begin{pmatrix} a_{11} & a_{12} & a_{13} \\ a_{21} & a_{22} & a_{23} \\ a_{31} & a_{32} & a_{33} \end{pmatrix} \begin{pmatrix} X \\ Y \\ Z \end{pmatrix}$$

where vectors $(a_{11}, a_{21}, a_{31})^T$, $(a_{12}, a_{22}, a_{32})^T$, and $(a_{13}, a_{23}, a_{33})^T$ make for an orthonormal basis. Thus, the camera coordinates can be expressed as follows:

$$\begin{aligned} &\left[(a_{11} - \alpha a_{31})x + (a_{12} - \alpha a_{32})y + (a_{13} - \alpha a_{33})z\right]^2 \\ &+\left[(a_{21} - \alpha a_{31})x + (a_{22} - \alpha a_{32})y + (a_{23} - \alpha a_{33})z\right]^2 \\ &= \gamma^2 (a_{31}x + a_{32}y + a_{33}z)^2 \end{aligned}$$

The part denote the focal length (i.e.orthogonal distance between O and Π_2) using the symbol f . Thus, the intersection Γ_2 of C and Π_2 is expressed as follows:

$$\begin{aligned} &(n^2 + k^2 - r^2)x^2 + 2(lk + np - rs)xy + (l^2 + p^2 - s^2)y^2 \\ &+2(km + nq - rt)x + 2(lm + pq - st) + m^2 + q^2 - t^2 \\ &= 0 \end{aligned}$$

where

$k = a_{11} - ta_{31}$

$n = a_{21} - sa_{31}$

$r = \gamma a_{31}$

$la_{12} - ta_2$

$p = a_{22} - sa_{32}$

$s = \gamma a_{32}$

$m = (a_{11} - ta_{31}) f$

$q = (a_{31} - sa_{33}) f$

$t = \gamma a_{33} f$

This equation shows that the projection is a quadratic curve, the geometrical interpretation of which can be a circle, hyperbola, parabola, or ellipse. In practice, due to a limited field of view, the projection will be a circle or ellipse. From this equation the center of the ellipse (u_c , v_c) can be expressed as follows:

$$u_c = \frac{(kl - nl)(lq - pm) - (ks - lr)(tl - ms) - (ns - pr)(wp - qs)}{(kp - nl)^2 - (ks - lr)^2 - (ns - pr)^2}$$

$$v_c \frac{(kl - nl)(mn - kq) - (ks - lr)(mr - kt) - (ns - pr)(qr - nt)}{(kp - nl)^2 - (ks - lr)^2 - (ns - pr)^2}$$

To determine the projection of the circle center, let us consider a situation in which the radius of the circle is zero; i.e., y = 0. This means that r, s, and t also become zero, and we obtain the position of the projected point due to the symmetry of the circle as well as the projection of the circle center (uc, vc), as follows:

$$u_0 = \frac{(lq - pm)}{(kp - nl)}$$
$$v_0 = \frac{(mn - kq)}{(kp - nl)}$$

In the case of a non-zero radius ($\gamma > 0$) there are some special cases in which the rotation is performed around the Z-axis (a31 = a32 = 0). Generally, can state that the center of the ellipse and projected center of the circle are not the same when applied to circular features with a non-zero radius.

In this study, we developed object-oriented programming software for a variety of vehicles and cameras. Finding a method by which to transform pixel values into actual parameters is the key to developing object-oriented programming software. Transforming the parameters requires that the scale of the image be derived from objects with known length. Paved roads generally lack objects by which to derive the scale. Thus, most existing PCI software measures the angle, elevation, and the pixel scale beforehand. The size of traffic signs, markings, and lights are strictly regulated; therefore, traffic markings can be used as objects from which to derive the image scale. Two axes in the images require adjustment: the X-axis and Y-axis. The distance between traffic marking is 4 m, and the width of the traffic lanes on national freeways is 3.75 m. Using the length and width of known objects enabled us to derive the following formula to transform images without being influenced by the angle or height from which the image was captured. The original image presents parallel lane markings, which are affected by the filming angle, such that extending the lines would cause them to intersect. Thus, Eq. 1 transforms the x-axis of the image into disjoint parallel lines, as follows:

$$F(x) = x.\left(1 + \frac{(x_0 - x_1)}{Y_0}\right).y$$

where x is the location of the pixel on the x-axis, x_0 indicates the bottom location of the lane marking on the x-axis, x_1 indicates the top location of the lane marking on the x-axis. L1 is the length of the first marking in the photo, and L2 is the length of the line at the bottom of the photo.

$$L_1 = l_0.N - \int_0^{L_1} d_y$$

$$L_2 = l_0.N - \int_L 2^{L_3} d_y$$

$$L_1 = L_2 = Markinglength\ FindlO$$

The next step involves associating each pixel i with the center of the nearest cluster, as shown in Fig. 4. This is the key to speeding up the algorithm, i.e., limiting the size of the search space in order to reduce computation time. In contrast, conventional k-means clustering would conduct a comparison of all cluster centers for every pixel. The search region in this study is an area 2S × 2S around the superpixel center. As shown in the CIELAB image, image pixels are assigned by the clustering cover, such that once the clustering is completed, the cluster centers are adjusted using the mean [L A B X Y] vector of the pixels belonging to that cluster. Thus, the cluster region can be considered a new segment of the image.

To summarize, the image is clustered into 200 segments, for use in executing the 2nd phase of K - means clustering, in which the image is clustered into three groups and presented in different colors. One of the colors is then identified as distress, depending on the area or the shape of the colored region.

Ensuring computational efficiency requires that a limit be placed on the number of images required for distress analysis and that the selection of images include only those that are likely to include indications of stress. Thus, we adopted a distress image filter using the RGB Standard Deviation (S.D.) of image segments as a standard. Sensitivity analysis of the image database involved grayscale processing of various parts of the image, marking the various colors to differentiate among blocks, and then analyzing the blocks indicative of damage. Thus, only images with an S.D. value exceeding 20 would be subjected to distress analysis; i.e., blocks indicative of major damage are larger than the others. The images are then clustered again. In this second-stage of K-means clustering, the basic unit of the image is the segments clustered in the first stage. Clustering is performed according to the mean LAB color value of every segment and the specified N2 value, which is generally 2 or 3. Overall, the purpose of clustering is to differentiate areas of distress from those that are in good condition.

To summarize, camera calibration is used to remove distortion, image scaling is derived from the length of known markers, and the ROIs are differentiated from areas presenting little indication of distress. The ROI is then subjected to automated superpixels recognition to extract evidence of distress.

2.4 Distress Type Classification

Once distress indicators are extracted from the image, they are identified as signs of Patching, Potholes, Alligator Cracking, or Manholes. Data pertaining to the distance, length, and region of the distress is then input into PCI. The areas of distress are initially separated into large-area distress (e.g., patching) and local distress (e.g., cracking) [8]. Classifying additional types of distress requires differentiation according to the ratio of vertical and horizontal distress segments. Crack connectivity is evaluated as follows: The Status Matrix is scanned block by block to find crack blocks. They are given corresponding id numbers and the length of the crack is added to the Length Table of the current branch. To improve recognition accuracy, after analyzing the damaged blocks in the photos, the software automatically retrieves the four previous and following photos and analyzes them for damage as well. . If only one neighbor shows signs of cracking, then the length of the crack is added to the corresponding items in the Length Table. Otherwise, proceed to the neighboring block and repeat the process. If more than one neighboring block shows signs of cracking, then select one of them to indicate the direction of the current branch and continue to check for further extension. As mentioned above, if the damaged part appear in multiple photos, then the damage progression and calculations are combined. If none of the neighboring blocks present indications of cracking, then the last block is treated as the end of the branch extension. If the length of the branch is shorter than a given threshold, then the branch is disregarded. The algorithm then finds the next candidate branch in the Branch Candidate Table, and repeats the extension check iteratively until the table is empty. The length of a crack is the sum of the length of all of the branches contributing to that crack. Finally, if the length of the crack is shorter than a given threshold, then it is not considered to be considered worthy of concern. The threshold for crack ck and branch length are adjusted according to the size of the window. In the literature, the threshold TC is calculated as follows:

$TC = 1.8s$

where S is the size of the window. Cracks are classified into three types: longitudinal, transverse, and alligator. The type of crack is determined by its angle measured against the horizontal axis (Ω) and the number of branches in the crack. Note that the angle is calculated according to the start and end points of each crack. If there are branches (regardless of the angle), then the crack is considered a block type.

3. RESULTS ANALYSIS AND DISCUSSION

3.1 Pavement Inspection Recording Database

This paper collected data from three types of major road in Taiwan. Our objective in this study was to enable the automatic analysis of road conditions from video segments without limitations in terms of the specific type of camera or vehicle used in the inspection.

3.2 Superpixels Reliability

This paper sought to determine the reliability of the proposed superpixels pavement detection application by conducting a comparison with semi-automatic image detection methods based on the manual identification of distress regions (via the human eye), which is the current inspection method in Taiwan. Fig. 4(a) presents an image showing an area of asphalt patching used in the performance comparison. The patching area is first examined by eye to verify that it is as an actual region of distress, whereupon the numbers of pixels in the region is calculated. The total number of pixels in Fig. 4(b) is 5,557,948 and the distress ratio is 39.26%. Fig. 4(c) presents the results of superpixels analysis, wherein the number of pixels in the region of distress in 14,155,776, resulting in a distress ratio of 39.15%. The variables in the superpixels are the initial clustering number N1 and the second clustering number N2. As shown in Table 1, a high clustering number does not have a positive effect on accuracy due to the effects of noise. Overall, the accuracy is ±2% of the true value, with the best performance achieved when N1 is 800 and N2 is 2. To account for the fact that the resolution of the dash cam is lower than that when capturing images from up close, this paper selected an N1 value of 100. Based on these comparison results, this paper determined that the best performance could be achieved by adopting an N1 value of less than 500. In subsequent analysis, this paper adopted an N1 value of 200.

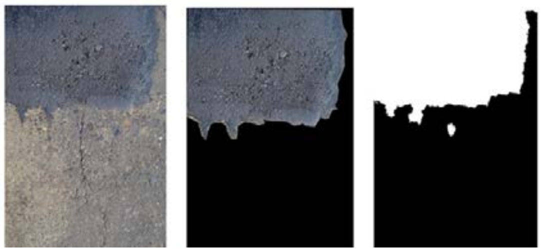

(a) (b) (c)

Fig.4 Indications of distress extracted using proposed superpixels application

3.3 Superpixels Comparison

In the following analysis, this paper focus on National Freeway No. 3, Guanxi Section (83km to 89km). Road conditions were evaluated using manual inspection, semi-automated inspection, and fully-automated inspection. Our primary objective in this study was to improve on current road inspection methods, the success of which is predicated on the ability to derive an accurate impression of road conditions through analysis of captured images.

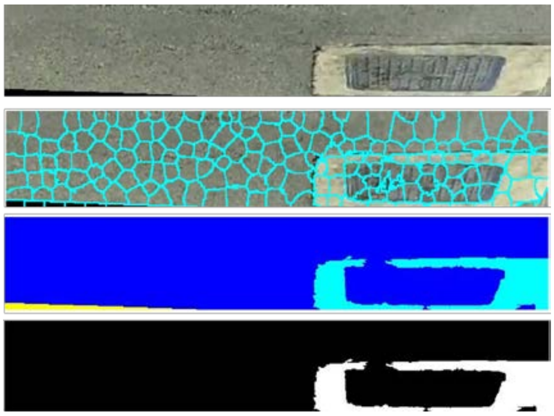

Fig.5 Images obtained using automated Superpixels recognition

A frame-rate of 60 FPS at a driving speed of 100 km/h would result in image spacing of 0.5 m. The length of the selected area is 4 m, which means that 15 images would be analyzed for each second of video, and 250 images would be required to cover a distance of 1 km. The spacing used in the NCU semi-automated inspection system is 25 m, which means that 40 images would be required to cover a distance of 1 km. Table 2 compares the quantity of distress regions and PCI values obtained using the three inspection methods, clearly indicating that the proposed Superpixels extraction scheme outperformed semi-automated extraction. Analysis of the 2nd Taiwan Provincial Rd. in Keelung, the three detection methods varied in the number of stress regions identified. This study adopted the values from manual inspection as the actual number of distress regions, for use as a reference in evaluating the performance of the fully-automated Superpixels scheme and the semi-automated NCU scheme. Table 3 indicates the quantity of patched areas, Ravels, potholes, and expansion joints. The proposed Superpixels scheme achieved the following coincidence rates: patched areas (91%), ravels (25%), potholes (100%), and expansion joints (100%). The wide image spacing used in the semi-automated scheme prevented the accurate detection of areas of distress.

Table 4 presents the analysis results from the 31th Taiwan Provincial Rd 235 (16km to 13 km). Automated Superpixels extraction identified 87.5% alligator cracks, 83.3% weathering and raveling, 77.8% patched areas, 66.7% potholes, and 55.6% long/trans cracking. Table 5 presents a comparison of automated Superpixels extraction and the semi-automated extraction in terms of distraction region. Clearly, the proposed scheme is effective in measuring the area of distress; however, the width of cracks cannot be derived due to limited resolution. In this analysis, five engineers were asked to identify various forms of distress based on visual acuity.

Using the average distress makes the automatic inspection method reproducible. The S.D. (σ) values were as follows: potholes (0.3%), patches (2.71%), and trans/long cracking (5.3), as shown in Table 6.

3.4 Software Development

In this study, Microsoft Visual C++ was used to combine the various functions of Matlab including video capture, image calibration, superpixels clustering, K-means clustering, distress classification, and PCI calculation. The user performs four actions: Step 1 – selection of road inspection video; Step 2 – camera calibration involving the selection of four traffic markers and image coordinates (Fig. 5); Step 3 – selection of analysis area; Step 4 – input of the frame interval based on driving speed and cutting number for superpixels clustering (200) and the number for K-Means Clustering (3).

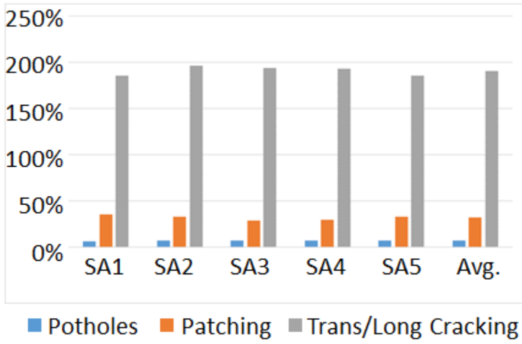

Fig. 6 True Ratio from Multiple Semi-Auto Selection

Finally, the SD value is input to enable the filtering out of unblemished areas in order to enhance processing efficiency.

4. CONCLUSION

The automated Superpixels extraction algorithm was shown to outperform conventional binary methods, as it requires only two parameter settings for image extraction. The proposed scheme opens the door to the fully-automated inspection of pavement conditions. A comprehensive view of the road surface can be obtained simply by adjusting the number of images captured from video sequences based on the driving speed. Six images per second is required for video obtained at 90 km/h (freeway driving), whereas four images are required for video obtained at 50 km/h (urban driving). SD values are used to differentiate between damaged and undamaged sections of road in order to enhance computational efficiency. The fact that the proposed Superpixels scheme has 95 percent confidence level with the semi-automatic distress recognition indicates the efficacy of using software as an alternative to current methods. The result in Taiwan

31th Provincial Road inspection could match 85.7

Table 1. Reliability of automated Superpixels extraction

Pieces	Distress pixel snumber	Total pixels number	Distress pixels rate	Accuracyy
300	4721480	14155776	0.34	98.97%
400	4836756	14155776	0.34	99.72%
500	5240733	14155776	0.37	98.81%
800	5139003	14155776	0.36	99.24%
1000	4951139	14155776	0.35	100.24%
1200	5076777	14155776	0.36	100.22%
1500	5179682	14155776	0.37	102.33%

Table 2. Methods Comparison

	Manual	NCU Semi-Auto	Auto-Superpixel
Numbers of image		40pic/km	7
Pothole	8	3	7M
Severity	5M+2H+1L	3M	54
PCI	43	71	74.4%
Accuracy		34.9%	

Table 3. Coincidence Rate Comparison in 2nd Taiwan Provincial Rd

	Patching	Ravels	Potholes	Expansion Joints
1.Man-eye	11	4	3	1
2.NCU Semi-Auto	5	1	1	1
3.Auto-Superpixel	10	1	3	1
Coincidence rate (1 vs 3)	91%	25%	1	1

Table 4. Detection Rate of automated Superpixels extraction algorithm

Distress Type	Alligator Cracking	Weathering & Raveling	Patching	Potholes	Long/Transs Cracking
Total	4	6	9	3	9
Check	3.5	5	7	2	5
	87.5%	83.3%	77.8%	66.7%	55.6%

Table 5. Comparison of extraction performance: Superpixels algorithm and manual inspection

Distress Type	1	19	11	13	10
Total	4	6	9	3	9
Check	3.5	5	7	2	5
	87.5%	83.3%	77.8%	66.7%	55.6%

Table 6. True Value from Multiple Semi-Auto Selection

Semi-Automated Selection	SA1	SA2	SA3	SA4	SA5	Avg.	
Potholes	6.2%	6.92%	7.08%	6.74%	6.56%	6.7%	0.3%
Patching	35.46%	33.18%	28.95%	29.66%	33.16%	32.08%	2.71%
Trans/Long Cracking	184.95	196.47	193.55	192.92	184.95	190.57	5.3

5. REFERENCES

[1] Sok S., Ouma Y.O., Hahn M., Miraliakbari A., Comparative Evaluation of Pavement Crack Detection Using Kernel-Based Technique in Asphalt Road Surfaces, Int. Arch. Photogramm. Remote Sens. Spat. Inf. Sci. XLI-B1, 2016, pp. 689-694.

[2] Construction and planning agency ministry of the interior, Urban Road Maintenance and Management Spec, Taipei, 2003.

[3] Wu Y., Zhu F., A rapid structural damage detection method using integrated ANFISand interval modeling technique, Appl. Soft Comput. 25 , 2014, pp.473-484.

[4] Liu B., Wei H., Dong Z., Hypercolumn-array based image representation and its application toshapebased object detection, Appl. Soft Comput. 52 , 2017, pp. 333-347.

[5] Balcones D, Marcos O., Llorca D.F., Sotelo M.A., Parra I., Ocaña M., Aliseda P., Yarza P., Amírola A., Gavilán M., Adaptive Road Crack Detection System by Pavement Classication, Sensors 11 , 2011, pp. 9628-9657.

[6] Massanet S., Bibiloni P., Hidalgo M.G., General-purpose curvilinear object detection with fuzzymathematical morphology, Appl. Soft Comput. 60 , 2017, pp.655-669.

[7] Jiji G.W., Linda C.H., Crack detection in X-ray images using fuzzy index measure, Appl. Soft Comput. 11, 2011, pp. 3571-3579.

[8] L. Ying, E. Salari, Beamlet Transform-Based Technique for Pavement Crack Detection and Classication, Comput-Aided. Civ. Inf. 25 , 2010, pp. 572-580.

[9] Gavilán M., Balcones D., Marcos O., Llorca D. F., Sotelo M.A., Parra I., Amírola A., Adaptive road crack detection system by pavement classification. Sensors, 11(10), pp. 9628-9657.

[10] Linda, C. H., and Jiji, G. W. (2011). Crack detection in X-ray images using fuzzy index measure. Applied Soft Computing, 11(4), 2011, pp. 3571-3579.

[11] Miraliakbari A., Sok S., Ouma Y. O. and Hahn M. Comparative Evaluation of Pavement Crack Detection Using Kernel-Based Techniques in Asphalt Road Surfaces. International Archives of the Photogrammetry, Remote Sensing and Spatial Information Sciences, 1, 2016.

[12] Wei H., Dong Z. and Liu B. Hypercolumn-array based image representation and its application to shape-based object detection. Applied Soft Computing, 52, 2017, pp. 333-347.

[13] Ying L. and Salari E.. Beamlet transform ‐ based technique for pavement crack detection and classification. Computer ‐ Aided Civil and Infrastructure Engineering, 25(8), 2010, pp.572-580.

[14] Zhu F. and Wu Y., A rapid structural damage detection method using integrated ANFIS and interval modeling technique. Applied Soft Computing, 25, 2014, pp. 473-484.